The Unusually Strong Hydrogen Bond between the Carbonyl of Q_A and His M219 in the *Rhodobacter sphaeroides* Reaction Center Is Not Essential for Efficient Electron Transfer from Q_A^- to Q_B[†]

Jacques Breton,*[,‡] Jérôme Lavergne,[§] Marion C. Wakeham,[||] Eliane Nabedryk,[‡] and Michael R. Jones[||]

Service de Bioénergétique, CEA-Saclay, 91191 Gif-sur-Yvette Cedex, France, UMR 6191 CNRS-CEA-Aix-Marseille II, DEVM-CEA-Cadarache, 13108 St Paul lez Durance, France, and Department of Biochemistry, School of Medical Sciences, University of Bristol, University Walk, Bristol, BS8 1TD, United Kingdom

Received January 12, 2007; Revised Manuscript Received March 22, 2007

ABSTRACT: In native reaction centers (RCs) from photosynthetic purple bacteria the primary quinone (Q_A) and the secondary quinone (Q_B) are interconnected via a specific His−Fe−His bridge. In *Rhodobacter sphaeroides* RCs the C_4═O carbonyl of Q_A forms a very strong hydrogen bond with the protonated N_π of His M219, and the N_τ of this residue is in turn coordinated to the non-heme iron atom. The second carbonyl of Q_A is engaged in a much weaker hydrogen bond with the backbone N−H of Ala M260. In previous work, a Trp side chain was introduced by site-directed mutagenesis at the M260 position in the RC of *Rb. sphaeroides*, resulting in a complex that is completely devoid of Q_A and therefore nonfunctional. A photochemically competent derivative of the AM260W mutant was isolated that contains a Cys side chain at the M260 position (denoted AM260(W→C)). In the present work, the interactions between the carbonyl groups of Q_A and the protein in the AM260(W→C) suppressor mutant have been characterized by light-induced FTIR difference spectroscopy of the photoreduction of Q_A. The Q_A^-/Q_A difference spectrum demonstrates that the strong interaction between the C_4═O carbonyl of Q_A and His M219 is lost in the mutant, and the coupled C⋯O and C⋯C modes of the Q_A^- semiquinone are also strongly perturbed. In parallel, a band assigned to the perturbation of the C_5-N_τ mode of His M219 upon Q_A^- formation in the native RC is lacking in the spectrum of the mutant. Furthermore, a positive band between 2900 and 2400 cm^{-1} that is related to protons fluctuating within a network of highly polarizable hydrogen bonds in the native RC is reduced in amplitude in the mutant. On the other hand, the Q_B^-/Q_B FTIR difference spectrum is essentially the same as for the native RC. The kinetics of electron transfer from Q_A^- to Q_B were measured by the flash-induced absorption changes at 780 nm. Compared to native RCs the absorption transients are slowed by a factor of about 2 for both the slow phase (in the hundreds of microseconds range) and fast phase (microseconds to tens of microseconds range) in AM260(W→C) RCs. We conclude that the unusually strong hydrogen bond between the carbonyl of Q_A and His M219 in the *Rb. sphaeroides* RC is not obligatory for efficient electron transfer from Q_A^- to Q_B.

Purple photosynthetic bacteria use light energy to generate a protonmotive force that supports bacterial growth and multiplication. Photochemical charge separation inside a membrane-bound pigment-protein complex called the reaction center (RC[1]) initiates a cycle of electron transfer reactions that are coupled to the translocation of protons across the cytoplasmic membrane. A key step in this process is the reduction of a dissociable secondary quinone at the so-called Q_B site in the RC by a permanently bound primary quinone at the so-called Q_A site. Reduction of the Q_A quinone is achieved by light-driven charge separation across the membrane dielectric, on a time scale of a few hundred picoseconds. The electron is then passed from Q_A^- to Q_B on a time scale of around 100 μs, forming a semiquinone at the Q_B site (see refs *1*−*3* for reviews). This reaction is multiphasic, with a fast phase in the 5 μs range and one or several slow phases in the tens to hundreds of microseconds (*1*, *4*). In isolated RCs with the native ubiquinone in the Q_A site the slower phase is dominant. This slower component appears to be gated by a conformational change that occurs in response to reduction of Q_A (*1*, *5*), with the result that the rate of the Q_A^- to Q_B reaction is independent of its driving force (*6*, *7*). In contrast the rate of the fast phase seen at elevated levels in RCs in chromatophores, and also in purified RCs with various naphthoquinones at the Q_A site, is dependent on the driving force and is not conformationally gated (*7*). Following a second transmembrane charge separation a second electron is passed from Q_A^- to Q_B^- in a

[†] This work has been supported by the Biotechnology and Biological Sciences Research Council of the United Kingdom (Grant B18667 to M.R.J. and M.C.W.).

* Corresponding author. SBE, CEA-Saclay, Bât. 532, 91191 Gif-sur-Yvette Cedex, France. Phone: 331 69082239. Fax: 331 69088717. E-mail: cadara3@dsvidf.cea.fr.

[‡] Service de Bioénergétique, CEA-Saclay.

[§] UMR 6191 CNRS-CEA-Aix-Marseille II, DEVM-CEA-Cadarache.

[||] University of Bristol.

[1] Abbreviations: RC, reaction center; IR, infrared; Q_A, primary quinone electron acceptor; Q_B, secondary quinone electron acceptor; P, primary electron donor.

10.1021/bi700057f CCC: $37.00
Published on Web 05/12/2007

reaction that is coupled to the uptake of a proton to form the state Q_BH^-. This second reduction occurs on a time scale of around 1 ms and is rapidly followed by the uptake of a second proton, forming a quinol (or dihydroquinone, denoted Q_BH_2) (see refs *2*, *3* for reviews). This quinol then detaches from the Q_B site for reoxidation in the cytochrome bc_1 complex, and the empty Q_B binding pocket is refilled by a quinone from the intramembrane quinone pool.

The two sequential electron transfer reactions between Q_A and Q_B have been subjected to extensive experimental analysis. A controversial topic is the nature of the conformational change that gates the dominant, slower phase of electron transfer from Q_A^- to Q_B in isolated RCs. The first evidence for this gating came from the observation that electron transfer from Q_A^- to Q_B is abolished in RCs frozen to cryogenic temperatures in the dark, but is retained in RCs frozen under continuous illumination (i.e., in the $P^+Q_B^-$ state, where P^+ is the photooxidized primary electron donor) and then returned to the ground state in a subsequent dark period (*5*, *8*). The interpretation of this is that the conformational change that gates electron transfer is locked out during freezing of RCs in the dark, but this conformational state is locked in during freezing of RCs in the $P^+Q_B^-$ state, and is then retained when the RCs subsequently relax to the ground state under dark, cryogenic conditions. A number of suggestions have been made concerning the nature of the gating conformational change, including changes in protonation state or hydrogen-bond pattern (*9*−*12*), a movement of the Q_B quinone inferred from crystallographic data (*13*−*16*), or a combination of the two with protonation or hydrogen-bond changes triggering Q_B movement (*17*−*19*). However as yet a consensus view has not arisen, and the subject remains controversial in the light of accumulating evidence that gating is not attributable to Q_B movement (see refs *16*, *20*−*24* and discussions therein). The binding of divalent ions to the RC seems to interfere with the conformational change, slowing Q_A^- to Q_B electron transfer (*25*, *26*), and Xu and Gunner have reported that the permissive and nonpermissive conformational states differ in terms of their intraprotein electrostatic field, suggesting differences in protonation or dipole conformation that stabilize Q_B^- in the permissive conformational state (*8*).

A second aspect that is poorly understood is the significance of the structure of the protein−cofactor system between the two quinone binding sites and the role, if any, of the network of bonding interactions that connect the Q_A and Q_B quinones and the intervening Fe atom. The structure of this region of the protein in the *Rhodobacter* (*Rb.*) *sphaeroides* RC is shown in Figure 1. When in the so-called "proximal" binding position (*13*) the two quinones are arranged in an approximately symmetrical manner around the axis of 2-fold (pseudo)-symmetry that runs through the core of the RC protein (indicated by the dotted line in Figure 1). The iron sits on this symmetry axis between the two quinones and is connected to each quinone via the side chain of a His, specifically His 219 of the M-polypeptide (M219) in the case of Q_A, and His 190 of the L-polypeptide (L190) in the case of Q_B. The iron is also ligated to two further His residues and receives a bidentate ligand from a Glu residue, forming a His_4−Fe−Glu complex at the interface of the L- and M-polypeptides (not shown). Despite extensive biophysical investigation of the RC, the structural

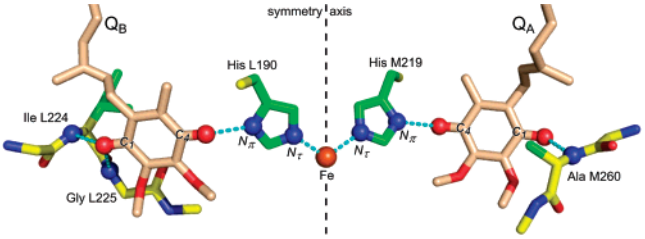

FIGURE 1: Interactions of Q_A and Q_B with the protein. The carbonyl groups of Q_A and Q_B engage in hydrogen bonds with the protein (cyan dots), and the two quinones are interconnected by a His−Fe−His bridge that straddles the axis of 2-fold symmetry (dashed line). Oxygen and nitrogen atoms are shown in red and blue, respectively, with atoms engaged in bonding interactions shown as spheres. Carbon atoms are shown in yellow for the protein backbone, green for side chains, and beige for the quinones.

and/or functional role of the His−Fe−His "bridge" that connects Q_A and Q_B quinones (Figure 1) is not fully clear. It has been established that the rate of the $Q_A^- \rightarrow Q_B$ reaction is essentially unchanged when the Fe^{2+} is replaced with other divalent metals (*27*), that it is slowed by a factor of only 2 when the Fe^{2+} is removed and not replaced (*27*), and that the Fe^{2+} does not undergo redox changes during $Q_A^- \rightarrow Q_B$ electron transfer (*28*). This demonstrates that the Fe^{2+} does not act as a redox intermediate or an indispensable conduit for electron transfer. On the other hand, the yield of $P^+Q_A^-$ is reduced by 50% in Fe-depleted RCs, an effect attributed to a ~50-fold decrease in the rate of electron transfer from the bacteriopheophytin to Q_A (*29*). According to recent calculations (*30*), Fe depletion is expected to cause a 220 mV downshift of the midpoint potential of Q_A (and a smaller effect, 80 mV, on Q_B), which would account for the slower electron transfer from bacteriopheophytin to Q_A. Another consequence of Fe depletion is to facilitate the double photoreduction of Q_A (*27*). Finally, it has been proposed that Fe^{2+} may play a structural role in the assembly and maintenance of a rigid structure of the RC protein (*31*).

Data from FTIR spectroscopy have established that the two carbonyl groups of Q_B engage in approximately equivalent moderate-strength hydrogen bonds with the surrounding protein. The infrared (IR) stretching frequency of both Q_B carbonyl groups is located at 1641 cm^{-1}, downshifted by 10−20 cm^{-1} from their frequency in aprotic solvent (*32*, *33*). As shown in Figure 1, the C_4═O group of Q_B is hydrogen-bonded to the protonated N_π nitrogen of His L190, while the C_1═O group is hydrogen-bonded to the backbone amide groups of Ile L224 and Gly L225. In contrast, the Q_A quinone shows a pronounced asymmetry in hydrogen bonding, with a remarkably strong downshift of the stretching frequency of the C_4═O carbonyl of Q_A to 1601 cm^{-1} (*34*−*36*). As discussed in a previous report (*34*), this downshift by 50−60 cm^{-1} compared to the carbonyl stretch frequency of ubiquinone in solution indicates a very strong hydrogen bond with the protonated N_π of His M219, with an estimated binding free energy of −6 to −8 kcal mol^{-1}. The C_1═O carbonyl of Q_A is in a suitable position to interact with the backbone amide of Ala M260, but this interaction does not result in a shift of the stretching frequency of this carbonyl group compared to solution. Thus, although the X-ray crystal structure indicates a symmetry in quinone-protein interactions between Q_B and Q_A, the IR data indicate markedly different patterns of hydrogen bonding. The hydrogen-bonding state of the semiquinones in the bacterial RC has

also been examined by EPR spectroscopy (*37*−*40*). Notably, an asymmetric hydrogen-bonding pattern with a stronger bond between the N_π−H group of His M219 and the C_4⋯O group of the Q_A^- semiquinone than that between the peptide NH group of Ala M260 and the C_1⋯O group of Q_A^- has been inferred from ESEEM and ENDOR data.

The functional significance of the very strong hydrogen bond between the C_4═O carbonyl of Q_A and His M219 and the broader significance of the His−Fe−His bridge connecting Q_A and Q_B are not understood. One indication that this strong hydrogen bond may be of functional importance is that it is also a feature of the Q_A plastoquinone in photosystem II complexes from spinach and cyanobacteria (*41*−*43*), and there is also inequality in the interactions of the Q_A menaquinone in the *Rhodopseudomonas (Rps.) viridis* RC (*44*). One suggestion for the *Rb. sphaeroides* RC is that a strong hydrogen bond between Q_A or Q_A^- and the protein could hold the quinone more rigidly in its binding pocket, influencing the rate of electron transfer through a reduction in reorganization energy (*1*). Still another possibility is that the two hydrogen atoms responsible for the interaction between the C_4═O carbonyl of both quinones and the His−Fe−His bridge are directly involved in a proton-assisted electron transfer reaction between Q_A and Q_B (*45*). In this respect mutations that would perturb the strong interaction between the His−Fe−His bridge and the C_4═O carbonyl of Q_A could bring new information on this topic.

As described in previous reports, the introduction of a Trp side chain in place of Ala at the M260 position in the *Rb. sphaeroides* RC results in a complex (denoted AM260W) that is completely devoid of the Q_A ubiquinone (*46*−*49*). This blocks electron transfer through the reaction center, and so the mutant bacterium is no longer capable of photosynthetic growth. A photochemically competent derivative of the AM260W mutant strain was subsequently isolated that contained a Cys side chain at the M260 position (denoted AM260(W→C)) as a result of a single nucleotide change (TGG→TGT) (*50*). Photoreduction of the Q_A ubiquinone was restored in this mutant, with a rate approximately 3-fold slower than in the wild-type RC (*46*). Molecular modeling suggested that the Cys side chain would not clash with the headgroup of Q_A and that a small overlap of the sulfur atom with the isoprenoid chain could be overcome by a minor repositioning of this chain (*50*).

In the present work, the interactions between the carbonyl groups of Q_A and the protein in this photosynthetically competent AM260(W→C) suppressor mutant have been characterized by light-induced FTIR difference spectroscopy of the photoreduction of Q_A. The Q_A^-/Q_A difference spectrum of the AM260(W→C) mutant indicated a drastic decrease in the strength of the interaction between Q_A and His M219. Despite this, electron transfer from Q_A^- to Q_B is still functional with a rate that is slowed by a factor of 2 to 5. These findings are discussed in the light of current theories on the role of the His−Fe−His bridge and the mechanism for gating of electron transfer between the quinones.

MATERIALS AND METHODS

Biological Material. Construction of the AM260(W→C) mutant strain has been described previously (*50*). All strains used in the present work lacked the LH1 and LH2 antenna proteins (*50*, *51*). Material for kinetic spectroscopy consisted of intracytoplasmic membranes prepared from *Rb. sphaeroides* cells grown under semiaerobic conditions in the dark, as described previously (*52*). RCs for FTIR spectroscopy were purified according to procedures described previously (*53*) and were suspended in a buffer consisting of 20 mM Tris/HCl (pH 8.0)/0.1% lauryldimethylamine oxide (LDAO).

FTIR Difference Spectroscopy. The preparation of RC samples for FTIR experiments involving the photoreduction of Q_A and Q_B has been described in refs *34* and *32*, respectively. For both native and mutant RCs, the photoreduction of Q_A was achieved in the presence of 100 mM potassium ferrocyanide, 10 mM sodium ascorbate, 100 mM Tris/HCl buffer (pH 8.0), and the Q_B inhibitor stigmatellin (2 mM) under saturating continuous illumination, using a Schott RG715 cutoff filter and a water filter to prevent heating of the sample. The Q_B^- state was generated under single turnover saturating flash excitation (Nd:YAG laser, 7 ns, 530 nm) in the presence of 50 mM potassium ferrocyanide, 10 mM *N*,*N*,*N*′,*N*′-tetramethyl-*p*-phenylenediamine (TMPD), 100 mM Tris/HCl buffer (pH 8.0), after reconstitution of the RCs with an approximately 10-fold excess of ubiquinone-6.

Steady-state light-induced Q_A^-/Q_A FTIR difference spectra (*34*) were recorded at 285 K using a Nicolet 860 spectrometer equipped with a MCT-A detector, a KBr beam splitter, and a gas-flow cryostat. Difference spectra were calculated from two data sets each consisting of 32 scans (acquisition time 20 s) recorded before and during continuous illumination. The Q_B^-/Q_B FTIR difference spectra were recorded at 285 K as previously described (*32*, *54*, *55*). For a given RC sample, these measurements were repeated over an approximately 24 h period and the difference spectra were averaged. Spectral resolution was 4 cm^{-1}.

Kinetics of Electron Transfer from Q_A^- to Q_B. The flash-induced absorption changes in the near-IR region were recorded with a Joliot-type spectrophotometer (*56*, *57*), at room temperature. In this apparatus, the absorption is sampled at discrete times with short (4 μs width) monochromatic flashes. The excitation light was provided by a 4 μs xenon flash through a Schott BG39 filter. The membranes were suspended in a medium containing 50 mM Tris/HCl (pH 7.5), 25 mM potassium chloride, 0.8 mM potassium ferricyanide, and 0.2 mM potassium ferrocyanide. This redox poise maintained cytochrome c_2 oxidized, preventing any significant reduction of P^+ over the 1 ms time range where the $Q_A^-Q_B \rightarrow Q_AQ_B^-$ kinetics were recorded. It also ensured the total reoxidation of Q_B^- during the 1 min interval between successive experiments. Despite the use of antenna deficient membranes, a fluorescence artifact caused by the tail of the actinic flash was present in the first 300 μs and was corrected for. Owing to this problem the first data point was taken at 30 μs after the actinic flash. The full extent of the $P^+Q_A^-$ signal was measured in the ms range in the presence of 10 μM stigmatellin, which blocks the electron transfer to Q_B.

RESULTS AND DISCUSSION

Comparison of Q_A and Q_A^- Vibrations in Native and AM260(W→C) Reaction Centers. In Figure 2 the light-induced Q_A^-/Q_A FTIR difference spectrum in native *Rb. sphaeroides* RCs in the characteristic 1800−1200 cm^{-1}

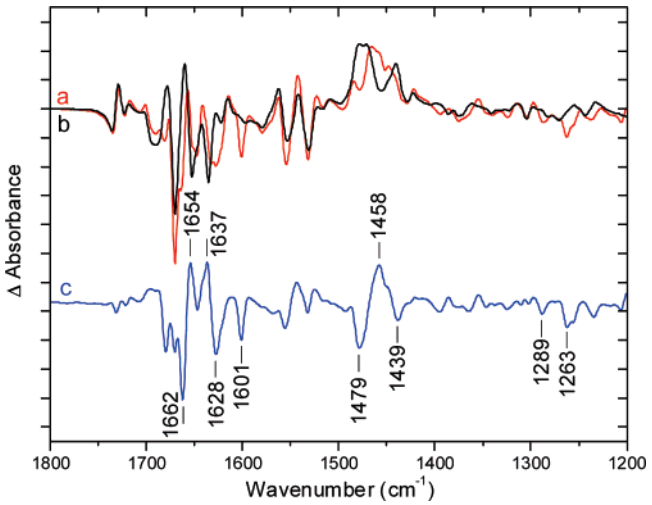

FIGURE 2: Light-induced Q_A^-/Q_A FTIR difference spectra at 285 K of purified RCs from *Rb. sphaeroides*. (a) Native RCs. (b) AM260(W→C) RCs. (c) Double-difference spectrum native-minus-AM260(W→C) calculated from spectra in Figure 2a and 2b. The tick marks on the vertical axis are separated by 4×10^{-4} absorbance unit. Frequencies are given $\pm$ 1 cm^{-1}.

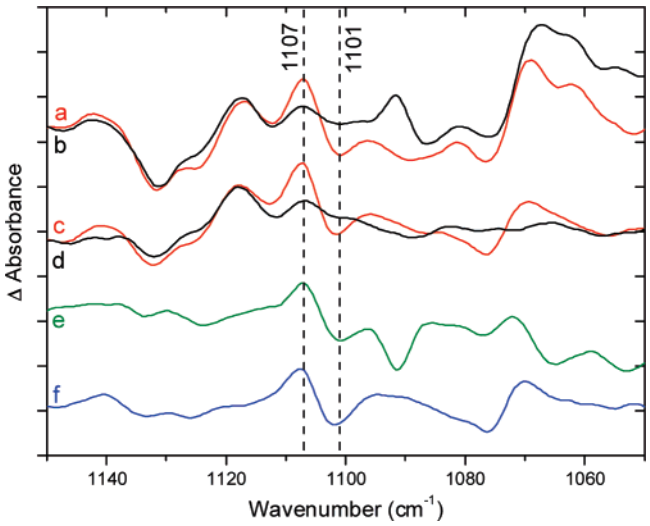

FIGURE 3: Light-induced Q_A^-/Q_A FTIR difference spectra of purified RCs from *Rb. sphaeroides*. (a,b) RCs from strain GR 0229, a strain deficient for His synthesis, grown in the presence of either unlabeled His (a) or uniformly ^{13}C-labeled His (b). (c) Native RCs. (d) AM260(W→C) RCs. (e) Double-difference spectrum unlabeled His-minus-^{13}C-labeled His calculated from spectra in Figure 2a and 2b. (f) Double-difference spectrum native-minus-AM260(W→C) calculated from spectra in Figure 2c and 2d. The tick marks on the vertical axis are separated by 1×10^{-4} absorbance unit.

frequency range (Figure 2a) is compared to that obtained under the same conditions with AM260(W→C) RCs (Figure 2b). Although the two spectra differed considerably, they had several features in common. Notably, they showed a similar pattern for the bands above 1700 cm^{-1} which have been assigned principally to the electrostatic response of the 10a-ester C═O vibrations of the bacteriopheophytin electron acceptor (*58*, *59*). Also, the bands corresponding to the main protein response to Q_A reduction, i.e., the large negative band at 1670 cm^{-1} (amide I) and the set of alternating positive and negative bands between 1570 and 1520 cm^{-1} (amide II), were common to both spectra. The observation that the amplitude of these bands was smaller in the difference spectrum of the AM260(W→C) mutant than in that of the native RC suggests a decreased magnitude of the protein response upon Q_A reduction in the mutant.

The C═O and C═C vibrational modes of Q_A and Q_A^- in native *Rb. sphaeroides* RCs have been identified in previous work (*34*−*36*, *60*). Using ubiquinone selectively labeled with ^{13}C at the C_1 or C_4 position, the carbonyl stretching frequencies of the neutral Q_A were identified at 1660 cm^{-1} for C_1═O and at 1601 cm^{-1} for C_4═O, with the latter mode strongly coupled to a C═C mode absorbing at 1628 cm^{-1} (*34*, *36*). The Q_A^-/Q_A difference spectrum of the AM260-(W→C) mutant (Figure 2b) showed that the bands previously assigned to the C═O and C═C vibrational modes of Q_A are highly perturbed compared to their positions in native RCs (Figure 2a). Notably, the three negative peaks or shoulders at 1601, 1628, and 1664 cm^{-1} present in the spectrum of native RCs were replaced by two new negative peaks at 1653 and 1636 cm^{-1} in the spectrum of the AM260(W→C) mutant (Figure 2b). This spectral alteration is best revealed in the native-minus-AM260(W→C) double-difference spectrum (Figure 2c), where a set of three negative bands at 1662, 1628, and 1601 cm^{-1} was replaced by two positive bands at 1654 and 1637 cm^{-1}. This observation points to a drastic change of the bonding interactions of Q_A in the AM260-(W→C) mutant compared to the situation in native RCs. In the absence of a Q_A^-/Q_A FTIR difference spectrum of the AM260(W→C) mutant reconstituted with selectively ^{13}C-labeled quinone, it was not possible to assign the 1637 cm^{-1} band to a moderately hydrogen bonded C═O group or to a C═C mode. However, the band at 1654 cm^{-1} corresponds to a C═O mode that is unperturbed compared to ubiquinone in solution (*60*). Previous work has established that the vibrational modes of the methoxy groups of Q_A give rise to bands at 1263 and 1286 cm^{-1} (*60*). These bands are strongly perturbed in the Q_A^-/Q_A FTIR difference spectrum of the AM260(W→C) mutant (Figure 2b), indicating a significant change in the conformation of the methoxy groups.

The vibrational modes of the Q_A^- semiquinone, that give rise to the cluster of three main positive bands at 1484, 1466, and 1448 cm^{-1} in the Q_A^-/Q_A difference spectrum of the native RC (Figure 2a), were strongly perturbed in the spectrum of the AM260(W→C) mutant (Figure 2b). Notably, the modes previously assigned to C_1⋯O at 1466 cm^{-1} and to C_4⋯O at 1448 cm^{-1} (*34*, *36*, but see *35* for a different assignment) were affected and gave rise to a broad band centered at 1475 cm^{-1} with a secondary peak at 1441 cm^{-1} in the spectrum of the AM260(W→C) mutant. The large changes observed in the absorption range of the C⋯O and C⋯C modes of Q_A^- (Figure 2) showed that the hydrogen bond between the N_π−H group of His M219 and the C_4⋯O group of the Q_A^- semiquinone has been significantly perturbed in the mutant complex. Notably, the upshift by 7−11 cm^{-1} of the C⋯C modes of Q_A^- is consistent with a weakening of the hydrogen bonds upon mutation. In this respect, it is interesting to note that the pattern of the C⋯O and C⋯C bands of Q_A^- in the AM260(W→C) mutant (Figure 2b) becomes more comparable to that observed in the Q_B^-/Q_B FTIR difference spectra of native RCs from *Rb. sphaeroides* (Figure 5b) and *Rps. viridis* which exhibit a main band at 1475−1479 cm^{-1} and a secondary peak at 1441−1445 cm^{-1} (*32*, *54*, *55*).

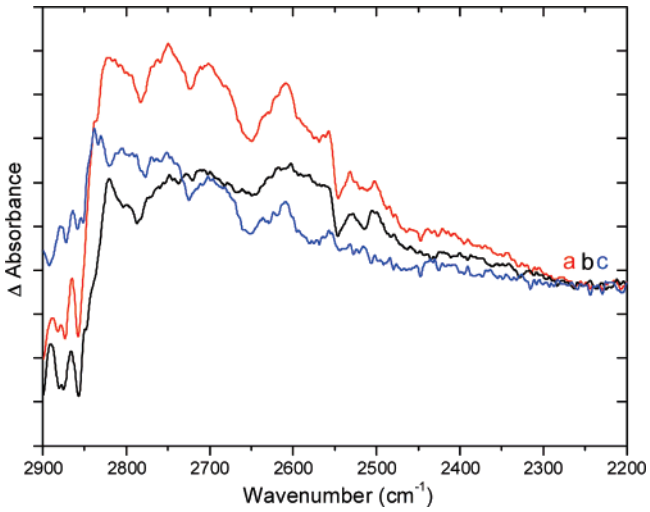

FIGURE 4: Light-induced Q_A^-/Q_A FTIR difference spectra at 285 K of purified RCs from *Rb. sphaeroides*. (a) Native RCs. (b) AM260(W→C) RCs. (c) Double-difference spectrum native-minus-AM260(W→C) calculated from spectra in Figure 2a and 2b. The tick marks on the vertical axis are separated by 1×10^{-5} absorbance unit.

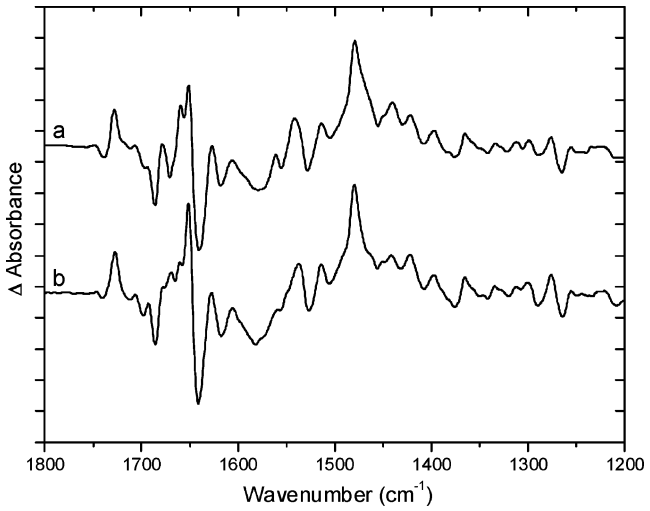

FIGURE 5: Light-induced Q_B^-/Q_B FTIR difference spectra at 285 K of purified RCs from *Rb. sphaeroides*. (a) AM260(W→C) RCs. (b) Native RCs. The tick marks on the vertical axis are separated by 1×10^{-4} absorbance unit.

Comparison of Histidine Vibrations in Native and AM260-(W→C) Reaction Centers. The C_5-N_τ mode of a His side chain protonated at N_π and coordinated to a metal at N_τ is expected to absorb in the frequency region around 1100−1110 cm^{-1} (*61*−*64*). The Q_A^-/Q_A FTIR difference spectra recorded with RCs isolated from a strain of *Rb. sphaeroides* deficient in the synthesis of histidine and grown in the presence of either unlabeled His or uniformly ^{13}C-labeled His (*65*) are reproduced in Figures 3a and 3b, respectively. This comparison reveals a 1107(+)/1101(−) cm^{-1} differential signal that has been assigned to perturbation of the $C_5-N_\tau H$ mode of His M219 upon Q_A^- formation in unlabeled RCs (Figure 3a) (*65*). On labeling with ^{13}C this differential signal downshifted to 1093(+)/1086(−) (Figure 3b).

In the present study, the 1107(+)/1101(−) cm^{-1} differential signal seen in the Q_A^-/Q_A FTIR difference spectrum of the native RCs (Figure 3c) was strongly suppressed in the spectrum of the AM260(W→C) mutant (Figure 3d). This suppression is obvious when comparing double-difference spectra. The spectrum in Figure 3f shows the effect of the AM260(W→C) mutation (native-minus-mutant), while the spectrum in Figure 3e shows the effect of suppressing the 1107(+)/1101(−) cm^{-1} differential signal by the ^{13}C isotopic downshift. These double-difference spectra are very similar as regards the position, shape, and magnitude of the 1107-(+)/1101(−) cm^{-1} differential signal. This observation is consistent with the removal of the strong hydrogen bond at the $C_4{=}O$ carbonyl of Q_A or Q_A^- with His M219 in the AM260(W→C) mutant.

The IR Continuum Bands in Native and AM260(W→C) Reaction Centers. The presence of broad positive bands extending between 2900 and 2400 cm^{-1} has previously been reported in the Q_A^-/Q_A and Q_B^-/Q_B FTIR difference spectra of *Rb. sphaeroides* and *Rps. viridis* RCs (*66*), as well as in the Q_A^-/Q_A spectrum of photosystem II (*42*, *66*). These bands downshift by 500−700 cm^{-1} upon $^1H/^2H$ exchange showing that they originate from protonated groups. These bands have tentatively been assigned to the electrostatic response, upon quinone photoreduction, of the Zundel polarizability (*67*, *68*) of protons fluctuating within a network of highly polarizable hydrogen bonds located in the surroundings of Q_A and Q_B (*66*). This network has been proposed to involve many amino acid residues as well as chains of ordered water molecules in the vicinity of the quinones, and it is envisaged that the protonation state of these water molecules changes upon arrival of the electron on the quinone. The positive amplitude of these bands in the Q_A^-/Q_A and Q_B^-/Q_B FTIR difference spectra suggests that the concentration and/or the polarizability of the protons in the network increases upon quinone reduction (*66*). On the other hand, the high proton polarizability which is responsible for these bands does not necessarily originate from charged protons (as in the Zundel cation $H_5O_2^+$) but may also be caused by localized strong hydrogen bonds. Indeed, similar broad bands with several sub-bands are observed in the 3000−2000 cm^{-1} frequency range for polycrystalline imidazole when the NH group is involved in strong hydrogen-bonding interactions (*42*, *69*, *70*).[2] In the case of the Q_A^-/Q_A spectrum of photosystem II, the bands in this region that are affected by ^{15}N labeling have been attributed to a His side chain strongly coupled to Q_A (*42*).

When the Q_A^-/Q_A FTIR difference spectrum of native RCs in the spectral range 2900−2200 cm^{-1} (Figure 4a) was compared to the spectrum of the AM260(W→C) mutant (Figure 4b), differences were found in the shape and substructure of these continuum bands. This is more clearly revealed in the native-minus-AM260(W→C) mutant double-difference spectrum (Figure 4c). It is thus likely that this difference arises mainly from the $N_\pi-H$ group of His M219 following loss of the strong hydrogen-bonding interaction with the $C_4{=}O$ carbonyl of Q_A. It is important to note that a large fraction of the broad continuum band observed in the spectrum of the native RC, more than one-half in terms of the area, was still present in the spectrum of the mutant RC (Figure 4b). This indicates that the continuum bands include contributions from protons other than that involved

[2] The N−H stretching mode of monomeric imidazole in carbon tetrachloride is observed at 3480 cm^{-1} (*71*).

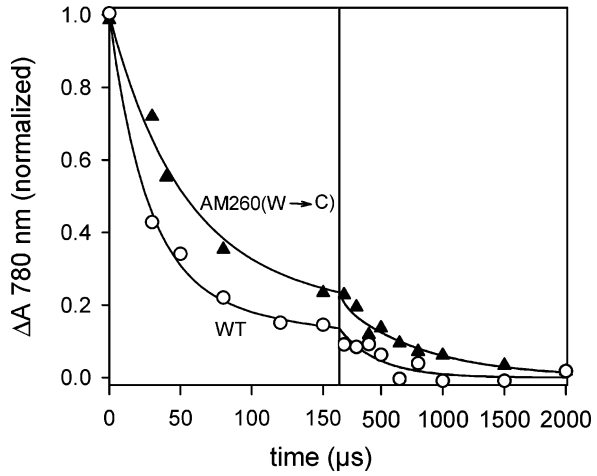

FIGURE 6: Time course of the flash-induced absorption changes at 780 nm associated with the $Q_A^-Q_B \rightarrow Q_AQ_B^-$ electron transfer in antennaless membranes containing native (open circles) or AM260(W→C) (closed triangles) RCs. The initial amplitude (data point at $t = 0$) was estimated independently from an experiment run in the presence of stigmatellin (see text). The offset corresponding to the P^+-P absorption change was subtracted, and the transients were normalized to their respective amplitudes. This amplitude was ~20% smaller in the mutant (on the basis of the P^+ change), which may be due to, e.g., a smaller Q_A^--induced electrochromic shift in the modified RC.

in the hydrogen bond between His M219 and Q_A. Furthermore, one cannot exclude that the modified spectrum of the mutant in this region may in part result from rearrangements that affect the hydrogen-bond network beyond the specific locale of the Q_A-His bond.

Limited Changes to the Q_B^-/Q_B Spectrum in AM260-(W→C) Reaction Centers. The Q_B^-/Q_B FTIR difference spectrum of AM260(W→C) RCs elicited by single turnover flash excitation (Figure 5a) was highly comparable to that of native RCs (Figure 5b) in both shape and amplitude. This shows preservation of the structural integrity at the Q_B site in the AM260(W→C) mutant. The main difference was the presence of a negative trough around 1670 cm^{-1} in the spectrum of the mutant. Although this additional signal is most probably related to the effect of the Ala to Cys mutation at position M260, it should be noted that the IR signals in the frequency region 1665−1670 cm^{-1} are particularly prone to variation in Q_B^-/Q_B FTIR difference spectra (*32*), and so it is unlikely that this negative signal reflected a significant change in structure of the Q_B site.

Kinetics of Electron Transfer from Q_A^- to Q_B. Because of the identical nature of the electron transfer partners, the $Q_A^-Q_B \rightarrow Q_AQ_B^-$ reaction causes no significant change in the absorbance spectrum of the quinones in the near-UV. However, the anionic semiquinones induce electrochromic shifts of the nearby bacteriopheophytin molecules on the A and B branches of the RC complex, which happen to have significantly distinct spectra in the near-IR region. The kinetics of the $Q_A^-Q_B \rightarrow Q_AQ_B^-$ reaction were followed from the absorption increase around 750 nm and decrease around 780 nm arising from these electrochromic shifts (*4*, *72*). Figure 6 shows the kinetics of the flash-induced absorption changes at 780 nm in antenna-deficient membranes containing either native or AM260(W→C) mutant RCs. The instrument used could not measure data points at times earlier than 30 μs after the flash, but the initial amplitude could be estimated by recording the flash-induced change in the millisecond range in the presence of stigmatellin, an inhibitor that blocks the electron transfer to Q_B. The lines in Figure 6 are two-exponential fits, taking this initial amplitude into account. The kinetics of the mutant RC were clearly slower than those of the native RC with ~2-fold larger half-times for both kinetic phases (18 μs → 35 μs and 221 μs → 476 μs) and a modest increase in the fraction of slow phase (22% → 26%), which is probably of marginal significance.

The fast phase in the kinetics of the native RC in particular was clearly poorly resolved because of the blind period of 30 μs. Tiede and co-workers (*4*) have reported the occurrence in chromatophores from *Rb. sphaeroides* of a large (64%) phase of the $Q_A^-Q_B \rightarrow Q_AQ_B^-$ reaction with $t_{1/2}$ ~6 μs which was present in the 750 nm (trough) region, but not in the 780 nm (peak) region. A similar fast electron transfer phase ($t_{1/2}$ ~4 μs), together with slower phases, was also monitored in the near-UV in RCs with a menaquinone substituted for Q_A (*1*). The interpretation proposed in these papers is that (i) the $Q_A^-Q_B \rightarrow Q_AQ_B^-$ electron transfer comprises two or three kinetic phases (from a few microseconds to several hundreds of microseconds) and (ii) the slower phases are accompanied with charge compensation events (e.g., proton uptake by the protonable groups in the Q_B region). In the near-IR electrochromic bands, it is proposed that the 750 nm changes respond both to the electron transfer and to charge compensation, while the 780 nm changes monitor only charge compensation (*4*). In the material used in the present study, the absorption changes in the trough region (around 750 nm) were very small, for unclear reasons, and we could not obtain reliable kinetic information in this region. Given this, if the 780 nm changes reflect charge compensation events rather than direct electron transfer, the kinetics of Figure 6 might underestimate the factor by which electron transfer is slowed in the mutant. Assuming that in native RCs the transient monitors a charge rearrangement (with $t_{1/2}$ ~18 μs) triggered by a $t_{1/2}$ ~6 μs electron transfer, and assuming further that this response (involving mainly the Q_B region) is not intrinsically slowed in the mutant, the slower 780 nm kinetics would mean that the electron transfer reaction has become slower than the rate-limiting step for charge rearrangement. Thus, the rate observed in the mutant would be close to the electron transfer rate, so that the electron transfer would change from $t_{1/2}$ ~6 μs in the native RC to ~35 μs in the mutant (considering only the fast phases). We therefore conclude, conservatively, that the electron transfer rate in the mutant is significantly slowed, by a factor in the range of 2 to 5.[3]

It has been reported that the ~6 μs (electron transfer only) phase and the slower components (electron transfer mixed with charge compensation) respond differently to modifications of the driving force ($-\Delta G_0$) (*7*). As expected for an electron transfer limited process, the fast phase is accelerated when increasing the driving force, but this is not the case for the slower phases, which appear to be "gated" by a conformational change (*6*, *7*). A plausible view is that the rapid phase reflects Q_A^- to Q_B electron transfer generating

[3] Additional experiments with isolated RCs and/or increased time resolution will be undertaken with the aim of clarifying whether the effect observed in the mutant is primarily due to a modified electron transfer rate or to a slower gating process.

a nonstabilized form of Q_B^-, while the slower phases correspond to progressive stabilization of Q_B^- (see ref *7* for a discussion). Still another view is that the fast phase reflects electron transfer to a subpopulation of Q_B already present in a favorable electrostatic configuration, while the slower phases correspond to changes of the electrostatic environment of the remaining population of Q_B (induced by the presence of Q_A^-) that would make it permissive for reduction. In these pictures, the gating mechanism would correspond to proton movements and/or conformational rearrangement of the protein rather than to the migration of the Q_B quinone from a distal to a proximal site proposed by Stowell et al. (*13*). Irrespective of the precise mechanism, the gating is believed to imply rearrangements in the Q_B region. Thus, if the modifications caused by the AM260(W→C) mutation are restricted to the Q_A region (but see below), they should affect the rate of electron transfer proper, rather than the gating. A slower electron transfer rate could arise from a decrease of the driving force ($-\Delta G_0$), an increase of the reorganization energy, or an increased distance between the cofactors. For example, according to ref *7* a more positive midpoint potential of Q_A by about 30 mV (70 mV) would account for a 2-fold (or 5-fold) slowing of the reaction; alternatively, a similar change in the reorganization energy would produce the same effect. If the effect is due to a modified distance between the quinones, displacements by 0.5 or 1.2 Å could account for the 2-fold or 5-fold change in rate, respectively.[4] On the other hand, the effect of the AM260(W→C) mutation may not be restricted to the Q_A region. Indeed, there are many observations suggesting interactions between the Q_A and Q_B regions so that it is plausible that this mutation could have repercussions extending to the Q_B pocket. This leaves open the possibility that the slower 780 nm transients could be due to a slowing of the gating process rather than a direct effect on the rate of ET. As noted above, the modifications of the continuum band in the 2900−2400 cm^{-1} region may be indicative of an effect on the hydrogen-bond network which can mediate the interaction between the two quinone regions.

CONCLUSION

As outlined in the introduction, the structural and/or functional role of the His−Fe−His "bridge" shown in Figure 1 remains unclear, but there is ongoing interest in this structural feature particularly in the context of how the Q_A^- → Q_B reaction is conformationally gated. A curious and unexplained feature of the His−Fe−His bridge is the unusually strong hydrogen bond between the C_4═O carbonyl of Q_A and the imidazole ring of His M219. In the present study it was established that this interaction is considerably weakened in the AM260(W→C) mutant, as evidenced by significant changes in the carbonyl vibrations of Q_A and Q_A^- and vibrational modes of His M219. Despite these changes, the rate of electron transfer from Q_A^- to Q_B is slowed by only a factor of 2 to 5 for the fast phase and of 2 for the slow phase in the AM260(W→C) RC, with no major changes in relative amplitude. This suggests that this very strong hydrogen bond is not of major functional relevance as regards electron transfer, but rather is probably a nuance of the precise conformation of the Q_A quinone in its binding pocket. This conformation may contribute to the maintenance of a low pK_a for the Q_A^- semiquinone, thus precluding the possibility of stabilization through protonation and double reduction to quinol. The changes in the rate of the Q_A^- → Q_B reaction observed in the mutant, if they reflect electron transfer rather than gating, are of a magnitude consistent with a small shift in the position of the Q_A quinone following replacement of the native Ala with the somewhat larger Cys, or a change in the electronic structure of the Q_A headgroup following introduction of the electronegative Cys side chain. Although there is no X-ray crystal structure available for the AM260(W→C) mutant at present, molecular modeling (*50*) has suggested that the Cys side chain can be accommodated in the Q_A binding pocket with only a minor steric clash between the sulfur atom of the Cys side chain and an atom of the isoprenoid chain of Q_A close to the point of attachment with the headgroup. This steric clash could be overcome by a very minor repositioning of the Q_A quinone in its binding pocket, which could account for the weakened hydrogen bond to His M219 and the modest changes in the rate of electron transfer to Q_A. Of course small changes in redox potential or reorganization energy caused by the electronegative Cys side chain could also in principle contribute to the observed rate changes.

Finally, formation of Q_A^- is accompanied by changes in proton vibrations, signified by a broad positive band between 2900 and 2400 cm^{-1} in the FTIR difference spectrum. The amplitude and line shape of this positive band was markedly altered in the spectrum of the AM260(W→C) mutant, suggesting that a significant proportion of the change in proton vibrations accompanying Q_A reduction involves the strong H-bond between the C_4═O group of Q_A and the N_π−H group of His M219 while a large fraction has a distinct origin, probably involving the network of highly polarizable hydrogen bonds located in the surroundings of Q_A and Q_B (*66*).

[4] Such relatively large displacements are unlikely (*50*), and the energetic effect appears more plausible.

REFERENCES

1. Li, J., Gilroy, D., Tiede, D. M., and Gunner, M. R. (1998) Kinetic phases in the electron transfer from $P^+Q_A^-Q_B$ to $P^+Q_AQ_B^-$ and the associated processes in *Rhodobacter sphaeroides* R-26 reaction centers, *Biochemistry 37*, 2818−2829.
2. Okamura, M. Y., Paddock, M. L., Graige, M. S., and Feher, G. (2000) Proton and electron transfer in bacterial reaction centers, *Biochim. Biophys. Acta 1458*, 148−163.
3. Wraight, C. A. (2004) Proton and electron transfer in the acceptor quinone complex of photosynthetic reaction centers from *Rhodobacter sphaeroides*, *Front. Biosci. 9*, 309−337.
4. Tiede, D. M., Utschig, L., Hanson, D. K., and Gallo, D. M. (1998) Resolution of electron and proton transfer events in the electrochromism associated with quinone reduction in bacterial reaction centers, *Photosynth. Res. 55*, 267−273.
5. Kleinfeld, D., Okamura, M. Y., and Feher, G. (1984) Electron transfer kinetics in photosynthetic reaction centers cooled to cryogenic temperatures in the charge-separated state: Evidence for light-induced structural changes, *Biochemistry 23*, 5780−5786.
6. Graige, M. S., Feher, G., and Okamura, M. Y. (1998) Conformational gating of the electron transfer reaction $Q_A^{-\bullet}Q_B \rightarrow Q_AQ_B^{-\bullet}$ in bacterial reaction centers of *Rhodobacter sphaeroides* determined by a driving force assay, *Proc. Natl. Acad. Sci. U.S.A. 95*, 11679−11684.
7. Li, J., Takahashi, E., and Gunner, M. R. (2000) $-\Delta G°_{AB}$ and pH dependence of the electron transfer from $P^+Q_A^-Q_B$ to $P^+Q_AQ_B^-$ in *Rhodobacter sphaeroides* reaction centers, *Biochemistry 39*, 7445−7454.

8. Xu, Q., and Gunner, M. R. (2001) Trapping conformational intermediate states in the reaction center protein from photosynthetic bacteria, *Biochemistry 40*, 3232−3241.
9. Beroza, P., Fredkin, D. R., Okamura, M. Y., and Feher, G. (1995) Electrostatic calculations of amino-acid titration and electron-transfer, $Q_A^-Q_B \rightarrow Q_AQ_B^-$, in the reaction-center, *Biophys. J. 68*, 2233−2250.
10. Alexov, E. G., and Gunner, M. R. (1999) Calculated protein and proton motions coupled to electron transfer: Electron transfer from Q_A^- to Q_B in bacterial photosynthetic reaction centers, *Biochemistry 38*, 8253−8270.
11. Xu, Q., and Gunner, M. R. (2002) Exploring the energy profile of the Q_A^- to Q_B electron transfer reaction in bacterial photosynthetic reaction centers: pH dependence of the conformational gating step, *Biochemistry 41*, 2694−2701.
12. Taly, A., Sebban, P., Smith, J. C., and Ullmann, G. M. (2003) The position of Q_B in the photosynthetic reaction center depends on pH: A theoretical analysis of the proton uptake upon Q_B reduction, *Biophys. J. 84*, 2090−2098.
13. Stowell, M. H. B., McPhillips, T. M., Rees, D. C., Soltis, S. M., Abresch, E., and Feher, G. (1997) Light-induced structural changes in photosynthetic reaction center: Implications for mechanism of electron-proton transfer, *Science 276*, 812−816.
14. Lancaster, C. R. D., and Michel, H. (1997) The coupling of light induced electron transfer and proton uptake as derived from crystal structures of reaction centres from *Rhodopseudomonas viridis* modified at the binding site of the secondary quinone, Q_B, *Structure 5*, 1339−1359.
15. Lancaster, C. R. D. (1998) Ubiquinone reduction and protonation in photosynthetic reaction centres from *Rhodopseudomonas viridis*: X-ray structures and their functional implications, *Biochim. Biophys. Acta 1365*, 143−150.
16. Kuglstatter, A., Ermler, U., Michel, H., Baciou, L., and Fritzsch, G. (2001) X-ray structure analysis of photosynthetic reaction center variants from *Rhodobacter sphaeroides*: Structural changes induced by point mutations at position L209 modulate electron and proton transfer, *Biochemistry 40*, 4253−4260.
17. Grafton, A. K., and Wheeler, R. A. (1999) Amino acid protonation states determine binding sites of the secondary ubiquinone and its anion in the *Rhodobacter sphaeroides* photosynthetic reaction center, *J. Phys. Chem. B 103*, 5380−5387.
18. Zachariae, U., and Lancaster, C. R. D. (2001) Proton uptake associated with the reduction of the primary quinone Q_A influences the binding site of the secondary quinone Q_B in *Rhodopseudomonas viridis* photosynthetic reaction centres, *Biochim. Biophys. Acta 1505*, 280−290.
19. Walden, S. E., and Wheeler, R. A. (2002) Protein conformational gate controlling binding site preference and migration for ubiquinone-B in the photosynthetic reaction center of *Rhodobacter sphaeroides*, *J. Phys. Chem. B 106*, 3001−3006.
20. Breton, J., Boullais, C., Mioskowski, C., Sebban, P., Baciou, L., and Nabedryk, E. (2002) Vibrational spectroscopy favors a unique Q_B binding site at the proximal position in wild-type reaction centers and in the Pro-L209→Tyr mutant from *Rhodobacter sphaeroides*, *Biochemistry 41*, 12921−12927.
21. Xu, Q., Baciou, L., Sebban, P., and Gunner, M. R. (2002) Exploring the energy landscape for Q_A^- to Q_B electron transfer in bacterial photosynthetic reaction centers: Effect of substrate position and tail length on the conformational gating step, *Biochemistry 41*, 10021−10025.
22. Breton, J. (2004) Absence of large-scale displacement of quinone Q_B in bacterial photosynthetic reaction centers, *Biochemistry 43*, 3318−3326.
23. Baxter, R. H. G., Ponomarenko, N., Srajer, V., Pahl, R., Moffat, K., and Norris, J. R. (2004) Time-resolved crystallographic studies of light-induced structural changes in the photosynthetic reaction center, *Proc. Natl. Acad. Sci. U.S.A. 101*, 5982−5987.
24. Baxter, R. H. G., Seagle, B. L., Ponomarenko, N., and Norris, J. R. (2005) Cryogenic structure of the photosynthetic reaction center of *Blastochloris viridis* in the light and dark, *Acta Crystallogr., Sect. D: Biol. Crystallogr. 61*, 605−612.
25. Utschig, L. M., Ohigashi, Y., Thurnauer, M. C., and Tiede, D. M. (1998) A new metal-binding site in photosynthetic bacterial reaction centers that modulates Q_A to Q_B electron transfer, *Biochemistry 37*, 8278−8281.
26. Paddock, M. L., Graige, M. S., Feher, G., and Okamura, M. Y. (1999) Identification of the proton pathway in bacterial reaction centers: Inhibition of proton transfer by binding of Zn^{2+} or Cd^{2+}, *Proc. Natl. Acad. Sci. U.S.A. 96*, 6183−6188.
27. Debus, R. J., Feher, G., and Okamura, M. Y. (1986) Iron-depleted reaction centers from *Rhodopseudomonas sphaeroides* R-26.1 - characterization and reconstitution with Fe^{2+}, Mn^{2+}, Co^{2+}, Ni^{2+}, Cu^{2+} and Zn^{2+}, *Biochemistry 25*, 2276−2287.
28. Hermes, S., Bremm, O., Garczarek, F., Derrien, V., Liebisch, P., Loja, P., Sebban, P., Gerwert, K., and Haumann, M. (2006) A time-resolved iron-specific X-ray absorption experiment yields no evidence for an $Fe^{2+} \rightarrow Fe^{3+}$ transition during $Q_A \rightarrow Q_B$ electron transfer in the photosynthetic reaction center, *Biochemistry 45*, 353−359.
29. Kirmaier, C., Holten, D., Debus, R. J., Feher, G., and Okamura, M. Y. (1986) Primary photochemistry of iron-depleted and zinc-reconstituted reaction centers from *Rhodopseudomonas sphaeroides*, *Proc. Natl. Acad. Sci. U.S.A. 83*, 6407−6411.
30. Ishikita, H., and Knapp, E.-W. (2006) Electrostatic role of the non-heme iron complex in bacterial photosynthetic reaction center, *FEBS Lett. 580*, 4567−4570.
31. Feher, G., and Okamura, M. Y. (1999) The primary and secondary acceptors in bacterial photosynthesis: II. The structure of the Fe^{2+}-$Q^{\bullet -}$ complex, *Appl. Magn. Reson. 16*, 63−100.
32. Breton, J., Boullais, C., Berger, G., Mioskowski, C., and Nabedryk, E. (1995) Binding-sites of quinones in photosynthetic bacterial reaction centers investigated by light-induced FTIRdifference spectroscopy: Symmetry of the carbonyl interactions and close equivalence of the Q_B vibrations in *Rhodobacter sphaeroides* and *Rhodopseudomonas viridis* probed by isotope labeling, *Biochemistry 34*, 11606−116.
33. Brudler, R., de Groot, H. J. M., van Liemt, W. B. S., Gast, P., Hoff, A. J., Lugtenburg, J., and Gerwert, K. (1995) FTIR spectroscopy shows weak symmetric hydrogen bonding of the Q_B carbonyl groups in *Rhodobacter sphaeroides* R26 reaction centers, *FEBS Lett. 370*, 88−92.
34. Breton, J., Boullais, C., Burie, J.-R., Nabedryk, E., and Mioskowski, C. (1994) Binding-sites of quinones in photosynthetic bacterial reaction centers investigated by light-induced FTIR difference spectroscopy: Assignment of the interactions of each carbonyl of Q_A in *Rhodobacter sphaeroides* using site-specific C-13-labeled ubiquinone, *Biochemistry 33*, 14378−14386.
35. Brudler, R., de Groot, H. J. M., van Liemt, W. B. S., Steggerda, W. F., Esmeijer, R., Gast, P., Hoff, A. J., Lugtenburg, J., and Gerwert, K. (1994) Asymmetric binding of the 1- and 4-C═O groups of Q_A in *Rhodobacter-sphaeroides* R26 reaction centers monitored by Fourier transform infra-red spectroscopy using site-specific isotopically labelled ubiquinone-10, *EMBO J. 13*, 5523−5530.
36. Breton, J., and Nabedryk, E. (1996) Protein-quinone interactions in the bacterial photosynthetic reaction center: Light-induced FTIR difference spectroscopy of the quinone vibrations, *Biochim. Biophys. Acta 1275*, 84−90.
37. Feher, G., Isaacson, R. A., Okamura, M. Y., and Lubitz, W. (1985) ENDOR of semiquinones in RCs from *Rhodopseudomonas sphaeroides*, in *Antennas and Reaction Centers of Photosynthetic Bacteria—Structure, Interactions and Dynamics* (Michel-Beyerle, M. E., Ed.) pp 174−189, Springer-Verlag, Berlin.
38. Bosch, M. K., Gast, P., Hoff, A. J., Spoyalov, A. P., and Tsvetkov, Yu. D. (1995) The primary acceptor Q_A in reaction centers of *Rhodobacter sphaeroides* R26 is hydrogen bonded to the $N^{\delta(1)}$-H of His M219. An electron spin echo study of Q_A^-, *Chem. Phys. Lett. 239*, 306−312.
39. Lubitz, W., and Feher, G. (1999) The primary and secondary acceptors in bacterial photosynthesis: III. Characterization of the quinone radicals by EPR and ENDOR, *Appl. Magn. Reson. 17*, 1−48.
40. Flores, M., Isaacson, R. A., Abrech, E., Calvo, R., Lubitz, W., and Feher, G. (2007) Protein-cofactor interactions in bacterial reaction centers from *Rhodobacter sphaeroides* R-26: II. Geometry of the Hydrogen bonds to the primary quinone $Q^{\bullet}{}_A^-$ by ^1H and ^2H ENDOR spectroscopy, *Biophys. J. 92*, 671−682.
41. Berthomieu, C., Nabedryk, E., Mäntele, W., and Breton, J. (1990) Characterization by FTIR difference spectroscopy of the photoreduction of the primary quinone acceptor Q_A in photosystem II, *FEBS Lett. 269*, 363−367.
42. Noguchi, T., Inoue, Y., and Tang, X.-S. (1999) Hydrogen bonding interaction between the primary quinone acceptor Q_A and a histidine side chain in photosystem II as revealed by Fourier transform infrared spectroscopy, *Biochemistry 38*, 399−403.
43. Rémy, A., Niklas, J., Kuhl, H., Kellers, P., Schott, T., Rögner, M., and Gerwert, K. (2004) FTIR spectroscopy shows structural

similarities between photosystems II from cyanobacteria and spinach, *Eur. J. Biochem. 271*, 563−567.
44. Breton, J. (1997) Efficient exchange of the primary quinone acceptor Q_A in isolated reaction centers of *Rhodopseudomonas viridis*, *Proc. Natl. Acad. Sci. U.S.A. 94*, 11318−11323.
45. Di Donato, M., Correa, A., and Peluso, A. (2003) The role of the iron-histidine bridge in the early steps of photosynthesis, *Chem. Phys. Lett. 369*, 549−555.
46. Ridge, J. P., van Brederode, M. E., Goodwin, M. G., van Grondelle, R., and Jones, M. R. (1999) Mutations that modify or exclude binding of the Q_A ubiquinone and carotenoid in the reaction center from *Rhodobacter sphaeroides*, *Photosynth. Res. 59*, 9−26.
47. McAuley, K. E., Fyfe, P. K., Ridge, J. P., Cogdell, R. J., Isaacs, N. W., and Jones, M. R. (2000) Ubiquinone binding, ubiquinone exclusion, and detailed cofactor conformation in a mutant bacterial reaction center, *Biochemistry 39*, 15032−15043.
48. Wakeham, M. C., Goodwin, M. G., McKibbin, C., and Jones, M. R. (2003) Photo-accumulation of the $P^+Q_B^-$ radical pair state in purple bacterial reaction centres that lack the Q_A ubiquinone, *FEBS Lett. 540*, 234−240.
49. Wakeham, M. C., Nabedryk, E., Breton, J., and Jones, M. R. (2004) Formation of a semiquinone at the Q_B site by A-branch or B-branch electron transfer in the reaction centre from *Rhodobacter sphaeroides*, *Biochemistry 43*, 4755−4763.
50. Wakeham, M. C., Frolov, D., Fyfe, P. K., van Grondelle, R., and Jones, M. R. (2003) Acquisition of photosynthetic capacity by a reaction centre that lacks the Q_A ubiquinone; possible insights into the evolution of reaction centres?, *Biochim. Biophys. Acta 1607*, 53−63.
51. Jones, M. R., Visschers, R. W., van Grondelle, R., and Hunter, C. N. (1992) Construction and characterisation of a mutant of *Rhodobacter sphaeroides* with the reaction centre as the sole pigment-protein complex, *Biochemistry 31*, 4458−4465.
52. Jones, M. R., Heer-Dawson, M., Mattioli, T. A., Hunter, C. N., and Robert, B. (1994) Site-specific mutagenesis of the reaction centre from *Rhodobacter sphaeroides* studied by Fourier transform Raman spectroscopy: Mutations at tyrosine M210 do not affect the electronic structure of the primary donor, *FEBS Lett. 339*, 18−24.
53. McAuley-Hecht, K. E., Fyfe, P. K., Ridge, J. P., Prince, S. M., Hunter, C. N., Isaacs, N. W., Cogdell, R. J., and Jones, M. R. (1998) Structural studies of wild type and mutant reaction centres from an antenna-deficient strain of *Rhodobacter sphaeroides*: Monitoring the optical properties of the complex from cell to crystal, *Biochemistry 37*, 4740−4750.
54. Breton, J., Berthomieu, C., Thibodeau, D. L., and Nabedryk, E. (1991) Probing the secondary quinone (Q_B) environment in photosynthetic bacterial reaction centers by light-induced FTIR difference spectroscopy, *FEBS Lett. 288*, 109−113.
55. Nabedryk, E., Breton, J., Hienerwadel, R., Fogel, C., Mäntele, W., Paddock, M. L., and Okamura, M. Y. (1995) Fourier transform infrared difference spectroscopy of secondary quinone acceptor photoreduction in proton transfer mutants of *Rhodobacter sphaeroides*, *Biochemistry 34*, 14722−14732.
56. Joliot, P., Béal, D., and Frilley, B. (1980) A new spectrophotometric method for the study of photosynthetic reactions. *J. Chim. Phys. 77*, 209−216.
57. Joliot, P., and Joliot, A. (1984) Electron-transfer between the 2 photosystems. 1. Flash excitation under oxidizing conditions, *Biochim. Biophys. Acta 765*, 210−218.
58. Breton, J., Nabedryk, E., Allen, J. P., and Williams, J. C. (1997) Electrostatic influence of Q_A reduction on the IR vibrational mode of the 10a-ester C═O of H_A demonstrated by mutations at residues Glu L104 and Trp L100 in reaction centers from *Rb. sphaeroides*, *Biochemistry 36*, 4515−4525.
59. Breton, J., Bibikova, M., Oesterhelt, D., and Nabedryk, E. (1999) Conformational heterogeneity of the bacteriopheophytin electron acceptor H_A in reaction centers from *Rhodopseudomonas viridis* revealed by Fourier transform infrared spectroscopy and site-directed mutagenesis, *Biochemistry 38*, 11541−11552.
60. Breton, J., Burie, J.-R., Berthomieu, C., Berger, G., and Nabedryk, E. (1994) The binding-sites of quinones in photosynthetic bacterial reaction centers investigated by light-induced FTIR difference spectroscopy: Assignment of the Q_A vibrations in *Rhodobacter sphaeroides* using ^{18}O- or ^{13}C-labeled ubiquinone and vitamin K_1, *Biochemistry 33*, 4953−4965.
61. Hasegawa, K., Ono, T.-K., and Noguchi, T. (2002) Ab initio density functional theory calculations and vibrational analysis of zinc-bound 4-methylimidazole as a model of a histidine ligand in metalloenzymes, *J. Phys. Chem. A 106*, 3377−3390.
62. Berthomieu, C., Boussac, A., Mäntele, W., Breton, J., and Nabedryk, E. (1992) Molecular-changes following oxidoreduction of cytochrome-b559 characterized by Fourier-transform infrared difference spectroscopy and electron-paramagnetic resonance−photooxidation in Photosystem-II and electrochemistry of isolated cytochrome-b559 and iron protoporphyrin-IX-bisimidazole model compounds, *Biochemistry 31*, 11460−11471.
63. Hienerwadel, R., and Berthomieu, C. (1995) Bicarbonate binding to the non-heme iron of Photosystem II investigated by Fourier transform infrared difference spectroscopy and ^{13}C-labeled bicarbonate, *Biochemistry 34*, 16288−16297.
64. Berthomieu, C., and Hienerwadel, R. (2001) Iron coordination in Photosystem II: Interaction between bicarbonate and the Q_B pocket studied by Fourier transform infrared spectroscopy, *Biochemistry 40*, 4044−4052.
65. Breton, J., Richaud, P., Verméglio, A., and Nabedryk, E. (2001) Infrared vibrational modes of histidine ligands of the primary electron donor and of Q_A in purple photosynthetic bacteria, in *PS2001 Proceedings of the 12th International Congress on Photosynthesis*, S7-002, CSIRO Publishing, Collingwood, Victoria, Australia.
66. Breton, J., and Nabedryk, E. (1998) Proton uptake upon quinone reduction in bacterial reaction centers: IR signature and possible participation of a highly polarizable hydrogen bond network, *Photosynth. Res. 55*, 301−307.
67. Zundel, G. (1992) Proton polarizability and proton transfer processes in hydrogen bonds and cations polarizabilities of other cation bonds. Their importance to understand molecular processes in electrochemistry and biology, *Trends Phys. Chem. 3*, 129−156.
68. Borgis, D., Tarjus, G., and Azzouz, H. (1992) An adiabatic dynamical simulation study of the Zundel polarization on strongly H-bonded complexes in solution, *J. Chem. Phys. 97*, 1390−1400.
69. Majoube, M., Millié, Ph., and Vergoten, G. (1995) Vibrational-spectra of 4-methylimidazole: Assignment of modes and calculation of Raman and resonance Raman intensities at the ab-initio 6-31G level, *J. Mol. Struct. 344*, 21−36.
70. Bellocq, A.-M., Perchard, C., Novak, A., and Josien, M.-L. (1965) Spectres de vibration de l'imidazole, de l'imidazole (D)-1, de l'imidazole (D3)-2,4,5 et de l'imidazole (D4) I: Région entre 4000 et 1700 cm^{-1}, *J. Chim. Phys. 62*, 1334−1343.
71. Perchard, C, and Josien, M.-L. (1965) Etude par spectroscopie infrarouge des vibrations de valence (NH) et (ND) de l'imidazole et du pyrazole (NH) et (ND), *J. Chim. Phys. 62*, 423−428.
72. Verméglio, A., and Clayton, R. K. (1977) Kinetics of electron transfer between the primary and the secondary electron acceptor in reaction centers from *Rhodopseudomonas sphaeroides*, *Biochim. Biophys. Acta 461*, 159−165.

BI700057F